AIP Advances

Emergent magnetic phase transitions in Fe-doped $SrTiO_{3-\delta}$

Cite as: AIP Advances **9**, 125302 (2019); https://doi.org/10.1063/1.5116671
Submitted: 26 June 2019 . Accepted: 14 November 2019 . Published Online: 03 December 2019

Yujuan Pei, Ruyi Zhang, Yang Song, Jiachang Bi, Wei Xu, Chen Zhou, Junxi Duan, Jingkai Yang, and Yanwei Cao

Emergent magnetic phase transitions in Fe-doped $SrTiO_{3-\delta}$

Cite as: AIP Advances 9, 125302 (2019); doi: 10.1063/1.5116671
Submitted: 26 June 2019 • Accepted: 14 November 2019 •
Published Online: 3 December 2019

Yujuan Pei,[1,2] Ruyi Zhang,[2] Yang Song,[2] Jiachang Bi,[2] Wei Xu,[2] Chen Zhou,[2] Junxi Duan,[3] Jingkai Yang,[1,a)] and Yanwei Cao[2,4,b)]

AFFILIATIONS

[1] State Key Laboratory of Metastable Materials Science and Technology, Yanshan University, Qinhuangdao 066004, China
[2] Ningbo Institute of Materials Technology and Engineering, Chinese Academy of Sciences, Ningbo, Zhejiang 315201, China
[3] School of Physics, Beijing Institute of Technology, Beijing 100081, China
[4] Center of Materials Science and Optoelectronics Engineering, University of Chinese Academy of Sciences, Beijing 100049, China

[a)] yangjk@ysu.edu.cn
[b)] ywcao@nimte.ac.cn

ABSTRACT

In defect engineering, both cation doping and oxygen vacancies play key roles in deciding the properties of oxide, and the utilization of their cooperation has attracted much interest in recent years. Here, we report an emergent magnetic phase transition near 18 K in Fe-doped $SrTiO_{3-\delta}$ by utilizing the magnetic interactions between the doped Fe cations and oxygen vacancies. The effects of Fe dopants and oxygen vacancies on the structural and magnetic properties were characterized by a high-resolution X-ray diffraction, Raman spectroscopy, and superconducting quantum interference device. In particular, as the temperature rises across the magnetic phase transition, the coercivity of Fe-$SrTiO_{3-\delta}$ decreases from ~7700 Oe at 2 K to ~104 Oe at 19 K. Our results of creating emergent magnetic phases with the coeffects of both cation dopants and oxygen vacancies could pave a way to inducing novel quantum states in epitaxial films on Fe-$SrTiO_{3-\delta}$ single crystal substrates with the magnetic proximity effect.

Defect engineering via creating, probing, controlling, and manipulating various kinds of defects in solid materials has provided a great platform to engineer novel functionalities and emergent quantum states,[1–5] for example, the key roles of precise control of dopants in modern semiconductors,[6–8] cuprate high-temperature superconductors,[9–12] colossal magnetoresistance manganites,[13] and magnetic topological insulators.[14–16] In particular, for the defect engineering in transition metal oxides, there are two main routes: cation doping and oxygen vacancy, the studies of which have attracted a large amount of and continuous interest recently.[5,17–19] Generally, cation dopants and oxygen vacancies play key roles in deciding the properties of oxide materials. However, the coeffects of the cation dopants and oxygen vacancies on magnetic properties in oxides remain elusive.

We take perovskite $SrTiO_3$ as an archetype to investigate the magnetic interactions of the cation dopants and oxygen vacancies in determining the emergent magnetic properties. The $SrTiO_3$ single crystals with a cubic symmetry (lattice parameters a = 3.905 Å) are widely used as substrates for the epitaxy of perovskite oxide films. In bulk, $SrTiO_3$ is paraelectric and diamagnetic at room temperature.[20] With a moderate cation doping (1%–40%), $SrTiO_3$ shows an emergent ferromagnetism (for Mn, Fe, and Co dopants),[21–25] an enhanced dielectric constant (for Mn dopant),[26] and a tunable anisotropic magnetoresistance (for Ni and Nb dopants),[27] which could be of great potential for oxide spintronics. With electron doping by oxygen vacancies, $SrTiO_3$ has been reported to show an insulator-to-metal transition, superconductivity, and even room temperature magnetism.[28–32] However, the magnetic properties of $SrTiO_3$ with coexisting magnetic cation dopants and oxygen vacancies are still unclear.

In this Letter, we focus on the magnetic properties of $SrTiO_3$ with coexisting magnetic cation dopants and oxygen vacancies. The magnetic contribution of both Fe dopants and oxygen vacancies in $SrTiO_3$ is investigated. The Fe-$SrTiO_{3-\delta}$ samples [see

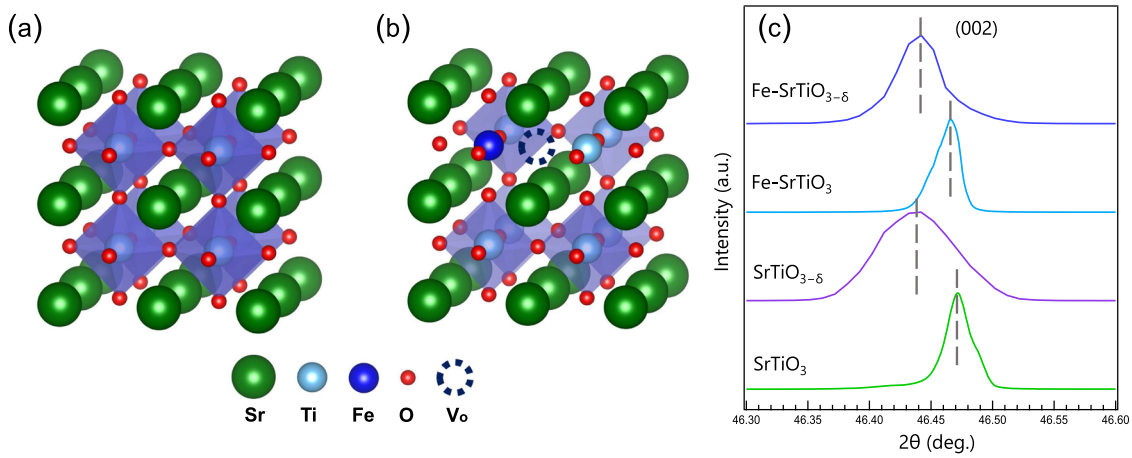

FIG. 1. Schematic representation of crystal structure of (a) pristine $SrTiO_3$ and (b) Fe-$SrTiO_{3-\delta}$ with coexisting Fe dopants and oxygen vacancies (dashed circle). (c) The 2theta-omega scans around the (002) diffractions of Fe-$SrTiO_{3-\delta}$, pristine Fe-$SrTiO_3$, $SrTiO_{3-\delta}$, and pristine $SrTiO_3$ single crystal samples.

Figs. 1(a) and 1(b)] were prepared by annealing Fe-$SrTiO_3$ single crystal in an ultrahigh vacuum (UHV). In contrast to the conventional paramagnetism in a cation doped Fe-$SrTiO_3$ and oxygen vacancies doped $SrTiO_{3-\delta}$, an unexpected magnetic phase transition emerges near 18 K in the Fe-doped $SrTiO_{3-\delta}$, demonstrating the contribution of the coexisting cation dopants and oxygen vacancies. Moreover, it is revealed that the coercive field and the line shapes of hysteresis loops strongly depend on temperature, indicating the complexity of this magnetic phase transition. Our work highlights the critical role of the coexisting Fe cation dopants and oxygen vacancies in engineering emergent magnetic phases.

The single crystalline (001)-oriented $SrTiO_3$ and 0.05% Fe-$SrTiO_3$ single crystals with the size of $5 \times 5 \times 0.5$ mm^3 were purchased from Hefei Kejing MTI corporation (China) and Shanghai Daheng Optics corporation (China), respectively. The samples were annealed in a UHV system equipped with a laser heater. The base pressure before laser annealing was kept below ~8.0×10^{-8} Torr. The temperature was kept at 1100 °C for 1 h during the laser-annealing, and the samples were quenched in UHV at room temperature afterward. The 2theta-omega scans around the (002) diffractions of all samples were performed on a PANalytical X'Pert Pro high-resolution X-ray diffractometer (HRXRD). Raman spectra ranging from 60 to 1000 cm^{-1} were collected with the Renishaw inVia Reflex confocal Raman spectroscopy. The field and temperature dependent magnetism were characterized by a superconducting quantum interference device (SQUID, Quantum Design). During the SQUID measurements, the external magnetic fields were always applied along [100] direction for all the samples to rule out the effect of inhomogeneities or any other structural factors. All measurements were repeated at least three times to make sure the results are repeatable.

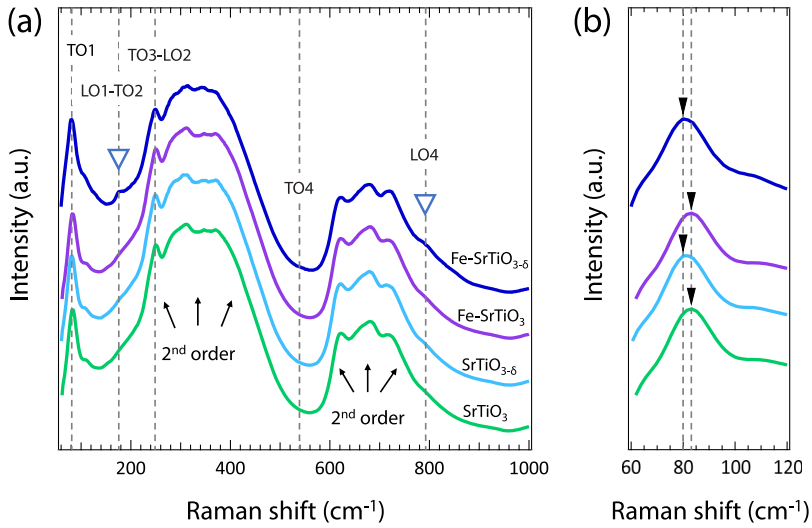

FIG. 2. (a) Raman spectra of Fe-$SrTiO_{3-\delta}$, pristine Fe-$SrTiO_3$, $SrTiO_{3-\delta}$, and pristine $SrTiO_3$ single crystal samples at the room temperature. (b) Magnified spectra near 80 cm^{-1} in (a) for clarity.

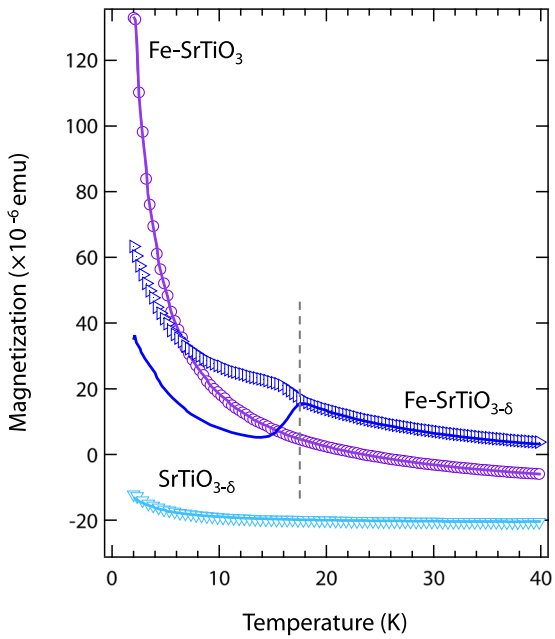

FIG. 3. M-T curves of Fe-$SrTiO_{3-\delta}$, pristine Fe-$SrTiO_3$, and $SrTiO_{3-\delta}$. During the zero-field-cooled (ZFC, solid lines) and field-cooled (FC, hollow symbols) measurements, the magnetic field was set at 2000 Oe along [100] orientation.

First, to investigate the effects of Fe dopants and oxygen vacancies on the crystal structures of pristine and laser-annealed samples, the XRD and Raman spectra were recorded. As shown in Fig. 1(c), both the (002) diffraction peaks of $SrTiO_3$ and Fe-$SrTiO_3$ after laser annealing shift toward small angles, indicating an expanding lattice parameter due to the induced oxygen vacancies.[33] The estimated lattice parameters for $SrTiO_{3-\delta}$ and Fe-$SrTiO_{3-\delta}$ are 3.908 Å and 3.907 Å, respectively, which are slightly larger than the lattice parameter ~3.905 Å of pristine $SrTiO_3$ and Fe-$SrTiO_3$ samples. Figure 2 shows that the peaks can be assigned as the Raman active modes of $SrTiO_3$.[34,35] Due to the centrosymmetry of $SrTiO_3$, the first-order Raman modes are forbidden, whereas the second-order Raman peaks are detectable. In Fe-$SrTiO_3$ single crystal, generally, the Fe^{4+} cations can replace the octahedron resided Ti^{4+} cations accompanied with oxygen vacancies to keep charge neutrality. The Fe^{4+} cations are Jahn-Teller distortive, which should break inversion symmetry and induce Raman active modes.[36–38] On the other hand, the presence of oxygen vacancies can destroy the integrity of octahedrons, resulting in first-order Raman peaks. However, solely doping Fe dopants or oxygen vacancies here are not strong enough to induce the first-order Raman peaks, which can be proved by the disappearance of the first-order modes in the Raman spectra of $SrTiO_{3-\delta}$ and Fe-$SrTiO_3$, as can be seen in Fig. 2(a). As a comparison, the coeffects of both Fe dopants and oxygen vacancies on Raman active peaks can be easily observed. The first-order LO1/TO2 mode (178 cm^{-1}) and LO4 mode (791 cm^{-1}) appear in the spectra of Fe-$SrTiO_{3-\delta}$ samples owing to inversion symmetry breaking. Apart from these apparent first-order modes, the shift of low-frequency band (80 cm^{-1}) toward lower wavenumbers in the spectra of $SrTiO_{3-\delta}$ and Fe-$SrTiO_{3-\delta}$ samples can be clearly viewed in Fig. 2(b), indicating a volume expansion of the unit cell caused by oxygen vacancies, which is consistent with the result from HRXRD in Fig. 1(c).[39,40]

Next, we characterize the magnetic properties of Fe-$SrTiO_{3-\delta}$ and the reference samples Fe-$SrTiO_3$ and $SrTiO_{3-\delta}$ by carrying out SQUID measurements. As seen in Fig. 3, the curves of zero-field-cooled (ZFC) and field-cooled (FC) modes are highly overlapped in both Fe-$SrTiO_3$ and $SrTiO_{3-\delta}$, whereas they separate and undergo a nonmonotonic change with a decreasing temperature from ~19 to 2 K in Fe-$SrTiO_{3-\delta}$. This phase transition arising from the coexisting Fe dopants and oxygen vacancies can be further revealed by the magnetization (M) vs magnetic field (H) curves measured across the transition temperature. As seen in Fig. 4(a), an obvious hysteresis loop with a large coercive field of ~7700 Oe can be observed at 2 K. However, with an increasing temperature, the hysteresis loops disappear and the coercive field decreases to a small value of ~92 Oe. Then, the hysteresis feature of Fe-$SrTiO_{3-\delta}$ resurfaces at 15 K, accompanied by a traceable coercive field of ~436 Oe. When the temperature further rises from 15 to 19 K, the coercive field

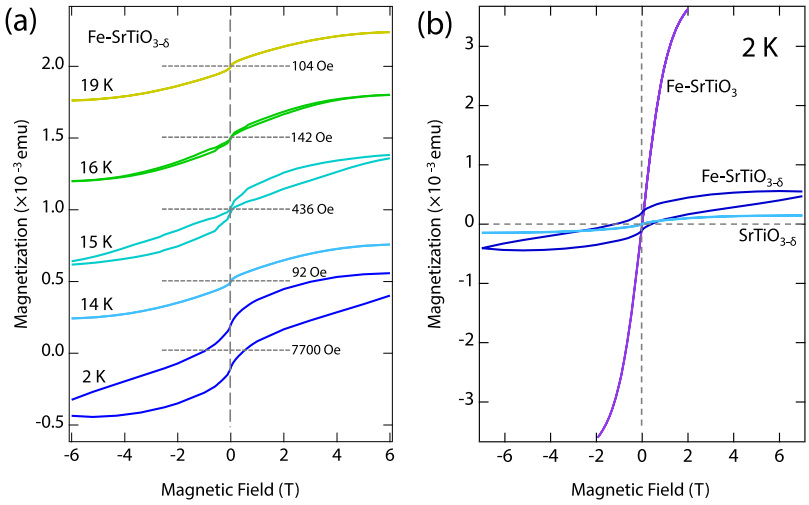

FIG. 4. (a) M-H hysteresis curves of Fe-$SrTiO_{3-\delta}$ along [100] direction at 2, 14, 15, 16, and 19 K. Temperature-dependent coercivities are labeled near each loop. (b) Comparison of M-H curves among Fe-$SrTiO_{3-\delta}$, pristine Fe-$SrTiO_3$, and $SrTiO_{3-\delta}$ at 2 K. For clarity, the linear diamagnetic backgrounds have been subtracted.

decreases once again and the hysteresis feature rises to ~102 Oe. Therefore, the temperature 15 K is near the turning point for hysteresis, which also corresponds to one of the minimum points of the ZFC curve in Fig. 3.

Finally, we discuss the origin of these emergent phase transitions. As seen in Fig. 4(a), the feature of obvious hysteresis with a small coercive field of M-H curve at 15 K is common in the magnetic systems consisting of two competing magnetic phases.[41,42] Moreover, it has been previously pointed out that site vacancies (particularly, oxygen vacancies) in the magnetic oxides can lead to nanoscale magnetic phase separations.[43,44] Therefore, the model of two competing magnetic phases with different magnetic orders and different responses to temperature/field can be established to explain the complicated evolution of M-T and M-H curves in Fe-$SrTiO_{3-\delta}$. In $SrTiO_{3-\delta}$ single crystal, a small amount of Ti^{3+} cations with unpaired $3d^1$ electronic configuration is produced owing to the existence of oxygen vacancies, which contribute to the weak ferromagnetism with a small coercivity (~270 Oe) shown in Fig. 4(b).[45] In a 0.05% Fe doped $SrTiO_3$ single crystal, Fe^{4+} cations in $3d^4$ configuration are separated in $SrTiO_3$, giving rise to a paramagnetic behavior with $M_S \sim 4\ \mu B$/Fe. In a Fe-$SrTiO_{3-\delta}$ single crystal, a large amount of oxygen vacancies is created after laser-annealing; they are high enough to provide electrons to a conduction band to drive Fe-$SrTiO_{3-\delta}$ into metallic states. The carrier density of a Fe-$SrTiO_{3-\delta}$ single crystal measured by the Hall effect is $5.76 \times 10^{18}/cm^{-3}$, surpassing the Mott criteria of $\sim 10^{18}/cm^{-3}$ for the metal-insulator transition.[47] Considering that each oxygen vacancy provides two electrons to the conduction band without any trapped charges, the minimum density of oxygen vacancies of $5.42 \times 10^{18}/cm^{-3}$ can be estimated. Actually, due to the trapped charges, the density of oxygen vacancies should be much higher than expected.[46] The hopping of polarons between Ti^{4+} and Ti^{3+} is responsible for the metallic behavior in a Fe-$SrTiO_{3-\delta}$ single crystal.[48] Therefore, many Fe^{4+} and Ti^{4+} cations are reduced to $Fe^{3+}$and Ti^{3+} cations, respectively, due to oxygen vacancies.[49] The strongly suppressed ferromagnetism (only 0.54 μB/Fe estimated from the M-H curves) in a Fe-$SrTiO_{3-\delta}$ single crystal suggests an antiparallel alignment of spins, which might arise from the superexchange between Fe^{3+} and Ti^{3+} cations. Then, a nanoscale magnetic separation involving one magnetic phase induced by Fe^{3+}-O^{2-}-Ti^{3+} and the other magnetic phase induced by unpaired spins in Ti^{3+} cations can be established. The complex involution of Fe-$SrTiO_{3-\delta}$ depending on field and temperature can be induced by these two magnetic phases, which might have a different phase transition temperature and coercive field.

In summary, an emergent magnetic phase transition near 18 K was observed in the Fe-doped $SrTiO_{3-\delta}$ with the presence of both Fe cations and oxygen vacancies. The effects of defects (Fe dopants and oxygen vacancies) on the structural and magnetic properties were characterized by Raman spectroscopy and SQUID, respectively, in the Fe-doped $SrTiO_{3-\delta}$ and reference samples, Fe-doped $SrTiO_3$ and $SrTiO_{3-\delta}$. Raman spectra revealed an obvious inversion symmetry breaking in the Fe-doped $SrTiO_{3-\delta}$ due to the coeffects of Fe dopants and oxygen vacancies. As the Fe-$SrTiO_{3-\delta}$ undergoes a magnetic phase transition, the coercivity increases from ~104 Oe at 19 K to ~7700 Oe at 2 K. Our results of creating the emergent magnetic phases by utilizing the coeffects of both cation dopants and oxygen vacancies could pave a route to designing novel quantum states in epitaxial films on Fe-$SrTiO_{3-\delta}$ single crystal substrates with the magnetic proximity effect.[50,51]

We acknowledge insightful discussions with G. Su, S. Zhang, and C. Liu. This work was supported by the National Natural Science Foundation of China (Grant No. 11874058), the Pioneer Hundred Talents Program of Chinese Academy of Sciences, the Ningbo 3315 Innovation Team, and the Ningbo Science and Technology Bureau (Grant No. 2018B10060). This work was partially supported by China Postdoctoral Science Foundation (Grant No. 2018M642500).

REFERENCES

[1] J. S. Park, S. Kim, Z. Xie, and A. Walsh, Nat. Rev. Mater. **3**, 194 (2018).
[2] H. L. Tuller and S. R. Bishop, Annu. Rev. Mater. Res. **41**, 369 (2011).
[3] Z. Lin, B. R. Carvalho, E. Kahn, R. Lv, R. Rao, H. Terrones, M. A. Pimenta, and M. Terrones, 2D Mater. **3**, 022002 (2016).
[4] R. Ramesh, Proc. Natl. Acad. Sci. U. S. A. **115**, 9344 (2018).
[5] J. Jeong, N. Aetukuri, T. Graf, T. D. Schladt, M. G. Samant, and S. S. P. Parkin, Science **339**, 1402 (2013).
[6] C. Gaul, S. Hutsch, M. Schwarze, K. S. Schellhammer, F. Bussolotti, S. Kera, G. Cuniberti, K. Leo, and F. Ortmann, Nat. Mater. **17**, 439 (2018).
[7] W. Prellier, A. Fouchet, and B. Mercey, J. Phys.: Condens. Matter **15**, R1583 (2003).
[8] M. Kisiel, O. O. Brovko, D. Yildiz, R. Pawlak, U. Gysin, E. Tosatti, and E. Meyer, Nat. Commun. **9**, 2946 (2018).
[9] P. A. Lee, N. Nagaosa, and X. Wen, Rev. Mod. Phys. **78**, 17 (2006).
[10] N. P. Armitage, P. Fournier, and R. L. Greene, Rev. Mod. Phys. **82**, 2421 (2010).
[11] B. Michon, C. Girod, S. Badoux, J. Kačmarčík, Q. Ma, M. Dragomir, H. A. Dabkowska, B. D. Gaulin, J. S. Zhou, S. Pyon, T. Takayama, H. Takagi, S. Verret, N. Doiron-Leyraud, C. Marcenat, L. Taillefer, and T. Klein, Nature **567**, 218 (2019).
[12] D. Dijkkamp, T. Venkatesan, X. D. Wu, S. A. Shaheen, N. Jisrawi, Y. H. Min-Lee, W. L. McLean, and M. Croft, Appl. Phys. Lett. **51**, 619 (1987).
[13] N. D. Mathur, G. Burnell, S. P. Isaac, T. J. Jackson, B. S. Teo, J. L. MacManus-Driscoll, L. F. Cohen, J. E. Evetts, and M. G. Blamire, Nature **387**, 266 (1997).
[14] R. Yu, W. Zhang, H. Zhang, S. Zhang, X. Dai, and Z. Fang, Science **329**, 61 (2010).
[15] C. Chang, J. Zhang, X. Feng, J. Shen, Z. Zhang, M. Guo, K. Li, Y. Ou, P. Wei, L. Wang, Z. Ji, Y. Feng, S. Ji, X. Chen, J. Jia, X. Dai, Z. Fang, S. Zhang, K. He, Y. Wang, L. Lu, X. Ma, and Q. Xue, Science **340**, 167 (2013).
[16] Y. Tokura, K. Yasuda, and A. Tsukazaki, Nat. Rev. Phys. **1**, 126 (2019).
[17] R. Mishra, Y. Kim, J. Salafranca, S. K. Kim, S. H. Chang, A. Bhattacharya, D. D. Fong, S. J. Pennycook, S. T. Pantelides, and A. Y. Borisevich, Nano Lett. **14**, 2694 (2014).
[18] J. M. D. Coey, Nat. Mater. **18**, 652 (2019).
[19] X. Zhu, J. Zhou, L. Chen, S. Guo, G. Liu, R. Li, and W. D. Lu, Adv. Mater. **28**, 7658 (2016).
[20] Y. Pai, A. Tylan-Tyler, P. Irvin, and J. Levy, Rep. Prog. Phys. **81**, 036503 (2018).
[21] M. Valant, T. Kolodiazhnyi, I. Arčon, F. Aguesse, A. Axelsson, and N. M. Alford, Adv. Funct. Mater. **22**, 2114 (2012).
[22] S. Middey, C. Meneghini, and S. Ray, Appl. Phys. Lett. **101**, 042406 (2012).
[23] J. He, X. Lu, W. Zhu, Y. Hou, R. Ti, F. Huang, X. Lu, T. Xu, J. Su, and J. Zhu, Appl. Phys. Lett. **107**, 012409 (2015).
[24] A. S. Tang, J. Pelliciari, Q. Song, Q. Song, S. Ning, J. W. Freeland, R. Comin, and C. A. Ross, Phys. Rev. Mater. **3**, 054408 (2019).
[25] D. Yao, X. Zhou, and S. Ge, Appl. Surf. Sci. **257**, 9233 (2011).
[26] D. Choudhury, S. Mukherjee, P. Mandal, A. Sundaresan, U. V. Waghmare, S. Bhattacharjee, R. Mathieu, P. Lazor, O. Eriksson, B. Sanyal, P. Nordblad, A. Sharma, S. V. Bhat, O. Karis, and D. D. Sarma, Phys. Rev. B **84**, 125124 (2011).

[27] A. Das, V. M. Goossens, A. S. Goossens, and T. Banerjee, paper presented at the Conference on Spintronics XI, San Diego, CA, 2018.
[28] S. Cook, M. T. Dylla, R. A. Rosenberg, Z. R. Mansley, G. J. Snyder, L. D. Marks, and D. D. Fong, Adv. Electron. Mater. **5**, 1800460 (2019).
[29] T. Taniuchi, Y. Motoyui, K. Morozumi, T. C. Rödel, F. Fortuna, A. F. Santander-Syro, and S. Shin, Nat. Commun. **7**, 11781 (2016).
[30] M. Altmeyer, H. O. Jeschke, O. Hijano-Cubelos, C. Martins, F. Lechermann, K. Koepernik, A. F. Santander-Syro, M. J. Rozenberg, R. Valentí, and M. Gabay, Phys. Rev. Lett. **116**, 157203 (2016).
[31] J. A. Bert, B. Kalisky, C. Bell, M. Kim, Y. Hikita, H. Y. Hwang, and K. A. Moler, Nat. Phys. **7**, 767 (2011).
[32] P. Moetakef, J. R. Williams, D. G. Ouellette, A. P. Kajdos, D. Goldhaber-Gordon, S. J. Allen, and S. Stemmer, Phys. Rev. X **2**, 021014 (2012).
[33] W. Gong, H. Yun, Y. B. Ning, J. E. Greedan, W. R. Datars, and C. V. Stager, J. Solid State Chem. **90**, 320 (1991).
[34] D. A. Tenne, I. E. Gonenli, A. Soukiassian, D. G. Schlom, S. M. Nakhmanson, K. M. Rabe, and X. X. Xi, Phys. Rev. B **76**, 024303 (2007).
[35] A. A. Sirenko, I. A. Akimov, J. R. Fox, A. M. Clark, H. Li, W. Si, and X. X. Xi, Phys. Rev. Lett. **82**, 4500 (1999).
[36] D. Ascienzo, O. Kurt, S. Greenbaum, T. J. M. Bayer, R. A. Maier, C. A. Randall, and Y. Ren, J. Am. Ceram. Soc. **101**, 2545 (2017).
[37] D. Ascienzo, O. Kurt, S. Greenbaum, T. J. M. Bayer, M. Russell, J. Wang, C. A. Randall, and Y. Ren, J. Am. Ceram. Soc. **102**, 4353 (2019).
[38] M. Vračar, A. Kuzmin, R. Merkle, J. Purans, E. A. Kotomin, J. Maier, and O. Mathon, Phys. Rev. B **76**, 174107 (2007).
[39] S. McIntosh, J. F. Vente, W. G. Haije, D. H. A. Blank, and H. J. M. Bouwmeester, Chem. Mater. **18**, 2187 (2006).
[40] W. S. Choi, H. K. Yoo, and H. Ohta, Adv. Funct. Mater. **25**, 799 (2015).
[41] P. Li, C. Xia, J. Li, Z. Zhu, Y. Wen, Q. Zhang, J. Zhang, Y. Peng, H. N. Alshareef, and X. Zhang, ACS Nano **11**, 5011 (2017).
[42] S. Xie, J. Cheng, B. W. Wessels, and V. P. Dravid, Appl. Phys. Lett. **93**, 181901 (2008).
[43] D. Zhu, Q. Cao, R. Qiao, S. Zhu, W. Yang, W. Xia, Y. Tian, G. Liu, and S. Yan, Sci. Rep. **6**, 24188 (2016).
[44] C. K. Xie, Y. F. Nie, B. O. Wells, J. I. Budnick, W. A. Hines, and B. Dabrowski, Appl. Phys. Lett. **99**, 052503 (2011).
[45] S. S. Rao, Y. F. Lee, J. T. Prater, A. I. Smirnov, and J. Narayan, Appl. Phys. Lett. **105**, 042403 (2014).
[46] C. Lin and A. A. Demkov, Phys. Rev. Lett. **111**, 217601 (2013).
[47] J. Wang, H. Huang, T. J. M. Bayer, A. Moballegh, Y. Cao, A. Klein, E. C. Dickey, D. L. Irving, C. A. Randall, and L. Chen, Acta Mater. **108**, 229 (2016).
[48] Y. Cao, S. Bhattacharya, J. Shen, C. A. Randall, and L. Q. Chen, J. Appl. Phys. **114**, 224102 (2013).
[49] Y. Zhang, O. Kurt, D. Ascienzo, Q. Yang, T. Le, S. Greenbaum, T. J. M. Bayer, C. A. Randall, and Y. Ren, J. Phys. Chem. C **122**, 12864 (2018).
[50] H. Zhang, X. Yan, H. Zhang, F. Wang, Y. Gu, X. Ning, T. Khan, R. Li, Y. Chen, W. Liu, S. Wang, B. Shen, and J. Sun, Phys. Rev. B **97**, 155150 (2018).
[51] H. Xue, Y. Hong, C. Li, J. Meng, Y. Li, K. Liu, M. Liu, W. Jiang, Z. Zhang, L. He, R. Dou, C. Xiong, and J. Nie, Phys. Rev. B **98**, 085305 (2018).